



Fast neurogenesis from carotid body quiescent neuroblasts accelerates adaptation to hypoxia

Verónica Sobrino^{1,2}, Patricia González-Rodríguez^{1,2}, Valentina Annese^{1,2}, José López-Barneo^{1,2,3,*}  & Ricardo Pardal^{1,2,**} 

Abstract

Unlike other neural peripheral organs, the adult carotid body (CB) has a remarkable structural plasticity, as it grows during acclimatization to hypoxia. The CB contains neural stem cells that can differentiate into oxygen-sensitive glomus cells. However, an extended view is that, unlike other catecholaminergic cells of the same lineage (sympathetic neurons or chromaffin cells), glomus cells can divide and thus contribute to CB hypertrophy. Here, we show that O₂-sensitive mature glomus cells are post-mitotic. However, we describe an unexpected population of pre-differentiated, immature neuroblasts that express catecholaminergic markers and contain voltage-dependent ion channels, but are unresponsive to hypoxia. Neuroblasts are quiescent in normoxic conditions, but rapidly proliferate and differentiate into mature glomus cells during hypoxia. This unprecedented “fast neurogenesis” is stimulated by ATP and acetylcholine released from mature glomus cells. CB neuroblasts, which may have evolved to facilitate acclimatization to hypoxia, could contribute to the CB oversensitivity observed in highly prevalent human diseases.

Keywords glomus cells; oxygen sensing; neural crest-derived stem cells; neuroblast proliferation and maturation; PNS niche

Subject Categories Neuroscience; Stem Cells

DOI 10.15252/embr.201744598 | Received 7 June 2017 | Revised 30 November 2017 | Accepted 13 December 2017 | Published online 15 January 2018

EMBO Reports (2018) 19: e44598

Introduction

Among the most striking, and as yet poorly understood, properties of the mammalian peripheral nervous system (PNS) are its ability to grow and regenerate. This is particularly evident in the carotid body (CB); a bilateral sensory organ located at the bifurcation of the carotid artery that, unlike other adult neural organs, can increase its size several folds in response to exposure to low environmental O₂ tension (PO₂). Despite the relevance of this

classical, homeostatic adaptive response, its underlying mechanisms have yet to be fully elucidated. The CB contains O₂-sensitive, neuron-like, glomus cells, which originate during embryogenesis from sympathoadrenal precursors that migrate from the neighboring superior cervical ganglion (SCG) [1]. In adult mammals, CB glomus cells behave as presynaptic-like chemoreceptor elements, which in response to hypoxia rapidly (in seconds) release transmitters to activate afferent fibers terminating in the brainstem respiratory center. This triggers fast cardiorespiratory reflexes (hyperventilation and sympathetic activation) to compensate for the lack of oxygen [2]. During exposure to sustained low PO₂, the CB grows and thereby increases the respiratory drive necessary for acclimatization to chronic hypoxemia, such as that occurring in high altitude dwellers [3–5] or in patients with obstructive pulmonary diseases [2,6]. However, CB over-activation, as seen in sleep apnea patients subjected to episodes of recurrent intermittent hypoxia [7] or in individuals with chronic heart failure (CHF) with decreased perfusion of the carotid region [8], can be maladaptive and cause exaggerated sympathetic outflow, thus leading to hypertension, peripheral insulin resistance, and metabolic syndrome [9]. CB hypertrophy is an indicator of poor prognosis in CHF patients [8,10], and denervation or pharmacological inhibition of the CB chemoreflex has been proposed to treat neurogenic refractory hypertension [7,11].

In recent years, significant experimental advances have provided an explanation for some of the main features of CB plasticity [12,13]. It has been shown that the adult mammalian CB is a neurogenic niche that, as neurogenic centers in the adult brain [14,15], contains a population of glia-like multipotent neural stem cells (NSCs), which upon activation by hypoxia can proliferate and differentiate into new neurons (glomus cells) and mesenchymal cell derivatives [12]. However, even though glomus cells are highly specialized chemosensory elements that are electrically excitable and contain dopamine, ATP, and several other neurotransmitters, an extended view is that they can proliferate during the early stages of acclimatization to chronic hypoxia [16–19]. This is an intriguing and as yet unexplained fundamental property of glomus cells that, if true, would distinguish them from other closely related neuronal cells (chromaffin cells in the adrenal

1 Instituto de Biomedicina de Sevilla (IBIS), Hospital Universitario Virgen del Rocío/CSIC/Universidad de Sevilla, Seville, Spain

2 Departamento de Fisiología Médica y Biofísica, Universidad de Sevilla, Seville, Spain

3 Centro de Investigación Biomédica en Red sobre Enfermedades Neurodegenerativas (CIBERNED), Seville, Spain

*Corresponding author. Tel: +34 955 923031; E-mail: lbarneo@us.es

**Corresponding author. Tel: +34 955 923038; E-mail: rpardal@us.es

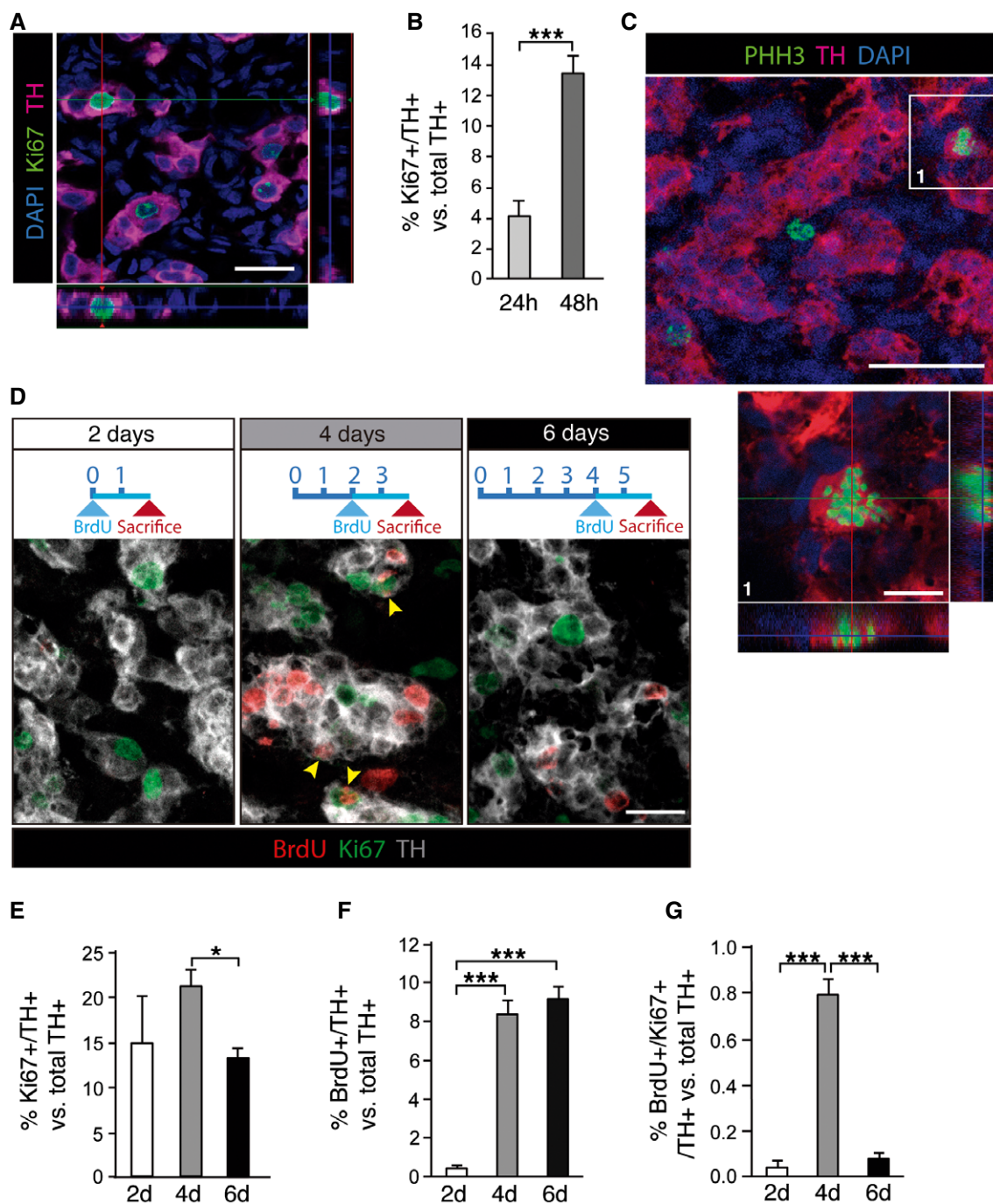


Figure 1. Proliferation of TH-positive adult CB cells.

- A** Immunohistochemical analysis of carotid body (CB) removed from rats subjected to hypoxia for 24 h. Image shows tyrosine hydroxylase (TH; red)-positive cells expressing the cell cycle marker Ki67 (green).
- B** Quantification of the frequency of proliferating CB TH⁺ cells after 24 and 48 h in hypoxia ($n = 4-6$ carotid bodies per time point).
- C** Confocal micrograph showing an example of a CB TH⁺ cell (red) in M phase of the cell cycle, thus accounting for its positivity to phosphorylated histone H3 (PHH3; green).
- D** Time course of CB TH⁺ (gray) cell proliferation, studied by Ki67 staining and BrdU incorporation during the 48 h prior sacrifice (see diagrams on top). Yellow arrowheads point to TH/Ki67/BrdU triple-positive cells.
- E-G** Quantifications of the time course experiment shown in (D), highlighting the transient nature of adult CB TH⁺ cell proliferation in response to chronic hypoxia ($n = 3-6$ carotid bodies per time point).

Data information: Scale bars: 20 μm in (A), 40 μm in (C), 10 μm in (C1), and 15 μm in (D). Data in bar graphs are presented as mean \pm SEM. * $P < 0.05$, *** $P < 0.001$ (Student's t -test).

Source data are available online for this figure.

medulla or sympathetic neurons), which do not show any proliferative capacity in adult life.

Herein we show that in contrast to commonly held beliefs, mature O₂-sensitive glomus cells do not proliferate. We have identified a subpopulation of rat glomus cells that are maintained in a quiescent, partially immature, status under normoxic conditions and which, upon exposure to hypoxia, divide and complete differentiation to form functionally mature O₂-sensitive cells in 24–48 h. We also show that this type of “fast neurogenesis” from pre-differentiated neuroblast-like cells, which is without precedent in other known neurogenic centers, can be modulated pharmacologically. Our findings shed light on as yet poorly understood features of CB adaptation to hypoxia, a classical chapter in oxygen homeostasis research. They also help to advance our understanding of the pathogenesis of highly prevalent comorbidities associated with CB over-activation and the development of potential therapeutic interventions.

Results

Hypoxia-induced proliferation of neuron-like CB glomus cells

Mammalian CB glomus cells are highly dopaminergic and can therefore be easily identified by tyrosine hydroxylase (TH) immunostaining. Exposure of rats to environmental hypoxia (10% O₂ tension) for a short time period (24 h) induced a population of TH-positive (TH⁺) cells to enter the cell cycle, as evidenced by the co-expression of TH and Ki67, a proliferation marker (Fig 1A). The number of proliferating TH⁺ CB cells drastically increased from ~4 to ~14% of the total TH⁺ cell population within the first 48 h in hypoxia (Fig 1B). This proliferative activity of TH⁺ cells disappeared when rats were returned to a normoxic (21% O₂ tension) environment (Fig EV1). TH⁺ cell proliferation in animals exposed to hypoxia was further documented by labeling the cells with an antibody against phosphohistone H3 (PHH3), a version of H3 histone that is only present in M phase of the cell cycle. This procedure resulted in characteristic images of TH and PHH3-double-positive cells lacking a nuclear membrane and exhibiting chromosome condensation (Fig 1C). Since Ki67 is a marker of the whole-cell cycle, the time course of cell divisions was studied by combining Ki67 with BrdU, which only labels cells that are at S phase of the cycle. By analyzing animals exposed to hypoxia for different time periods, and that had received BrdU during the last 48 h before sacrifice (Fig 1D), we observed that cell division in the neuronal (TH⁺) compartment was fast and transient, and maximal after 3–4 days of exposure to hypoxia (Fig 1E–G). After the first 3–4 days under hypoxia, the small percentage of BrdU and Ki67 double-positive cells (Fig 1G) indicates a clear exit from the cell cycle, being the majority of proliferative TH⁺ cells already post-mitotic after the first 6 days of exposure to hypoxia. The presence of a significant number of Ki67/TH double-positive cells at 6 days (Fig 1E) might represent the capacity of some of these cells to maintain proliferation beyond the first burst of neuronal cell division. These data indicate the existence of a transient period of fast and intense neurogenesis (generation of new TH⁺ glomus cells) in the CB due to division of pre-existing TH⁺ cells.

Identification and prospective isolation of dividing TH⁺ cells

Among the several cell surface markers tested, we found that the human natural killer-1 (HNK-1) membrane epitope, which is typically described in neural crest-derived cells [20,21], specifically labels the subset of TH⁺ cells with proliferation capacity in response to hypoxia (Fig 2A and B). The proliferation of TH⁺/HNK⁺ cells was confirmed in studies in which flow cytometry and time-lapse microscopy video imaging were used. Figure 2C (top panel) shows a typical flow cytometry dot plot from a dispersed normoxic rat CB after intracellular staining with antibodies against Ki67 and TH, combined with cell membrane staining with antibodies against HNK-1 (see Materials and Methods). Highly TH⁺ cells were negative for HNK-1 (red dots), while a subclass of moderately stained TH⁺ cells (mTH⁺ cells, green dots) were highly HNK⁺. We also observed a population of HNK⁺ cells, with medium to low expression of HNK-1 but negative for TH (blue dots), whose nature was not studied (TH-/HNK low cells). Exposure of the animals to hypoxia (48 h) drastically increased the number of proliferating (Ki67⁺) mTH⁺/HNK⁺ cells, thus indicating that they are the subpopulation of dividing glomus cells (Fig 2C and D).

As intracellular immunocytochemistry with anti-TH antibodies can only be performed in permeabilized fixed cells, we developed a procedure for sorting the two subclasses of TH⁺ live cells (TH⁺/HNK⁻ and mTH⁺/HNK⁺) by flow cytometry. We first found that TH⁺ (HNK⁻) cells are larger in size than mTH⁺/HNK⁺ cells [see Forward Scatter (FSC) axis in the plot in Fig EV2A]. Moreover, TH⁺ cells contain abundant mitochondria and other organelles [4], which make them more autofluorescent compared to bulk cells in the cytometer (FL-2 axis in the dot plot of Fig EV2B). Therefore, by using physical parameters and the cell membrane marker HNK-1, we were able to sort highly enriched (> 90%) populations of both mTH⁺/HNK⁺ and TH⁺ live cells (see Fig EV2B and C). When sorted cells were cultured and recorded for 48 h with time-lapse microscopy, cell division activity was observed in ~7% of mTH⁺/HNK⁺ cells maintained in normoxia (Nx); this value increased up to 46% in cells exposed to hypoxia (Hx) (*n* = 131 recorded cells). In contrast, cell division activity was rarely observed (< 3%) in sorted TH⁺ cells (*n* = 138 recorded cells), with such isolated cases of cell division probably due to incomplete separation of the sorted populations (Fig 2E and F). Taken together, these data strongly suggest that within the population of neuron-like glomus cells, hypoxia selectively triggers the proliferation of mTH⁺/HNK⁺ cells.

mTH⁺/HNK⁺ cells are immature glomus cells that complete differentiation during hypoxia

To further characterize the nature of mTH⁺/HNK⁺ cells, we used flow cytometry to study the dynamics of this population during long-lasting exposures to hypoxia (Fig 3). In normoxia, HNK-1 labels about one-third of all TH⁺ cells (Nx; Fig 3A). During the long-term exposure of rats to a hypoxic environment (Hx 5d and 21d in Fig 3B–D), we observed marked changes in the mTH⁺/HNK⁺ population, consisting of an evident increase in the expression of TH (encoded by a well-known hypoxia-inducible gene), which was even more pronounced than that in TH⁺ (HNK⁻) cells (Fig 3B), and a parallel decrease in HNK-1 expression to appear progressively similar to the TH⁺ (HNK⁻) population (Fig 3A–D).

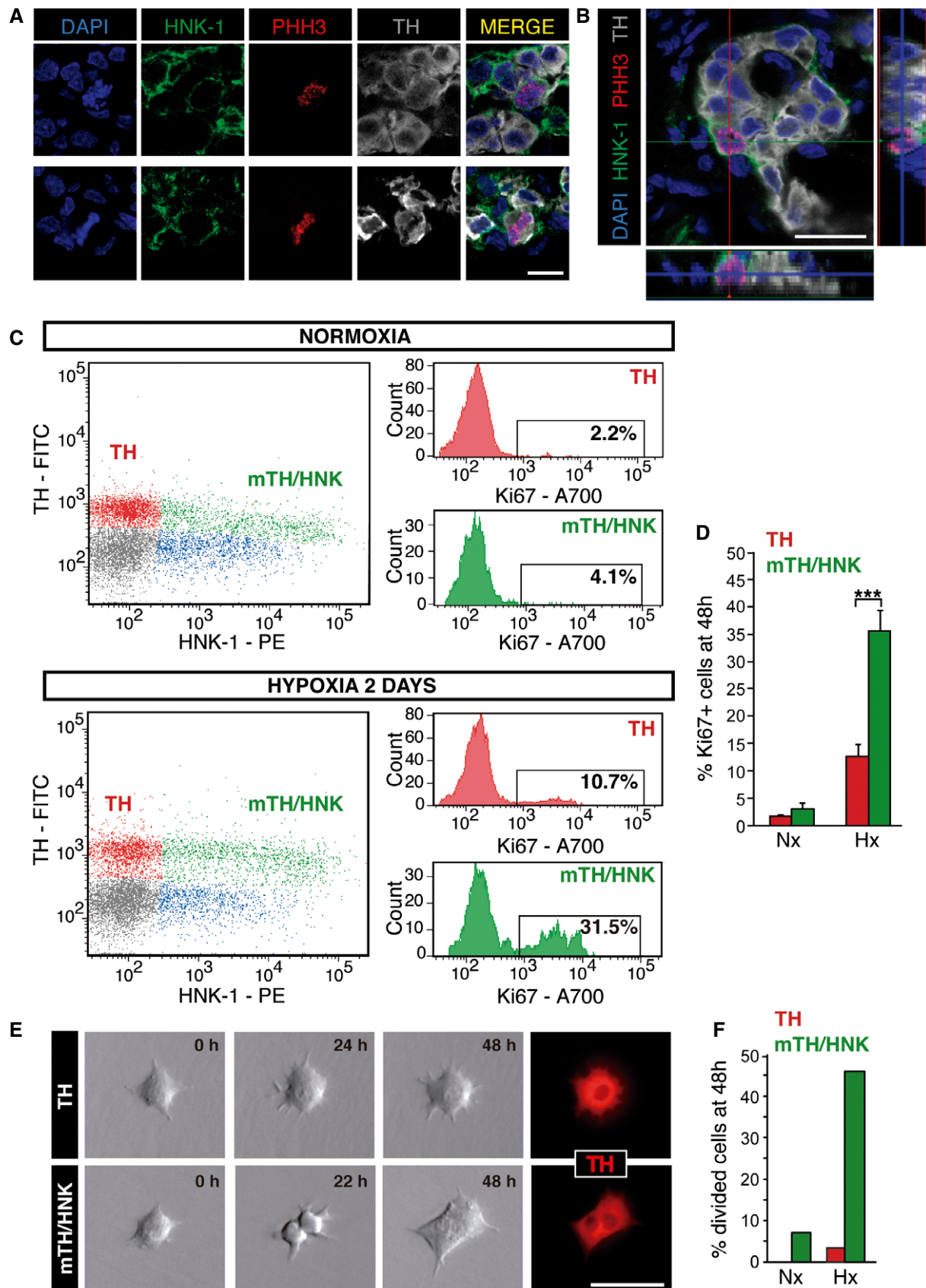


Figure 2.

Figure 2. HNK-1 specifically labels proliferating TH-positive CB cells.

- A, B Immunohistochemical analysis of CB from rats exposed to hypoxia for 48 h, illustrating the membrane expression of the glycoepitope HNK-1 in PHH3⁺ proliferating CB neuronal (TH⁺) cells.
- C Flow cytometry analysis of normoxic and 2d hypoxic CBs, with membrane staining of the cells with antibodies against HNK-1 and intracellular staining with antibodies against TH and Ki67. Note that upon exposure to hypoxia proliferation (Ki67⁺) is particularly increased in the HNK-1⁺ subpopulation of neuronal (TH⁺) cells.
- D Quantification of proliferating cells in flow cytometry plots as those shown in (C) ($n = 5$ normoxic, Nx, and 6 hypoxic, Hx, rats).
- E Time-lapse video microscopy imaging of TH⁺ and mTH⁺/HNK-1⁺ CB cells, sorted alive by flow cytometry (see Fig EV2). After 48 h recording, most cell division activity was observed in the HNK-1⁺ subpopulation.
- F Quantification of cell divisions observed after 48 h using time-lapse microscopy, confirming that proliferation is a feature of HNK-1⁺ CB neuronal cells [$n = 42$ TH⁺ and 42 mTH⁺/HNK⁺ cells exposed to normoxia (Nx; $n = 3$ rats), and 96 TH⁺ and 89 TH⁺/HNK⁺ cells exposed to hypoxia (Hx; $n = 5$ rats)].
- Data information: Scale bars: 10 μm in (A), 20 μm in (B), and 25 μm in (E). Data in bar graph of panel (D) are presented as mean \pm SEM. Data in bar graph of panel (F) are presented as the sum of dividing cells among total cells studied. *** $P < 0.001$ (Student's t -test). Source data are available online for this figure.

After 21 days in hypoxia, almost all the mTH⁺/HNK⁺ cells had disappeared (Fig 3C and D). Keeping in mind that TH is the rate-limiting enzyme in dopamine synthesis and hence constitutes a typical marker for mature neuronal cells in the CB, the data suggest that mTH⁺/HNK⁺ cells are pre-differentiated neuroblasts that upon exposure to hypoxia proliferate transiently and then rapidly complete maturation into fully differentiated glomus cells. The immature phenotype of mTH⁺/HNK⁺ cells was also corroborated by flow cytometry based on the expression of Tuj1, a neuroblast marker [22]. As expected, CB mTH⁺/HNK⁺ cells expressed higher levels of Tuj1 than TH⁺ (HNK⁻) mature neuronal cells (Fig 3E and F). Finally, as we have previously shown that mature glomus cells are larger in size than CB neuroblasts (Fig EV2A), the maturation process was confirmed by showing an increase in neuroblast cell size and a decrease in HNK-1 expression upon *in vitro* exposure to hypoxia (Fig EV3A–C).

To characterize the structural features of CB neuroblasts (mTH⁺/HNK⁺ cells) *in situ*, we performed electron microscopy (EM) studies using antibodies against HNK-1 conjugated to gold particles. As this technique has relatively low sensitivity, it favors the analysis to be focused on mTH⁺/HNK⁺ cells since they are the cells that are most positive for the expression of this surface marker in the CB (see Figs 2C and 3A). Nevertheless, we also observed some HNK low cells (Fig 4H), probably corresponding to the uncharacterized TH-/HNK low cells (blue dots in Fig 2C), which were not included in our EM analysis. The representative ultrastructural features of HNK⁺ neuroblasts in comparison with mature glomus cells, which are profusely characterized by EM in the literature [23,24], are shown in Fig 4A and B. Neuroblasts (green) were consistently smaller in size and contained patches of gold particles around their plasma membrane (arrows), confirming the high level of HNK-1 expression in these cells (Fig 4A). In contrast, mature glomus cells (red), which were not marked by gold particles (negative for HNK-1 staining), were easily identified by their larger size and by the presence of abundant secretory vesicles next to the plasma membrane (Fig 4B). mTH⁺/HNK⁺ cells also contained secretory vesicles (blue arrows in Fig 4C1), but these were smaller in size and fewer in number compared to mature glomus cells (Fig 4C–E). Within the typical CB cell clusters (glomeruli), mTH⁺/HNK⁺ neuroblasts were usually seen at the periphery and often separated by extracellular space from mature glomus cells, which were situated in the center (Fig 4F; see also Fig 4G for a quantification of the differences in the location of glomus

cells and neuroblasts within the CB glomeruli). However, cell-to-cell contacts, with a narrow intercellular cleft and associated electron-dense membrane zones, were occasionally observed between the two cell types (see yellow arrowheads in Fig 4C1), suggesting some type of communication between these cells. The structural arrangement of neuroblasts at the borders of glomeruli could indicate that when mTH⁺/HNK⁺ cells are activated by hypoxia *in vivo*, they mature into glomus cells to either expand the size of the glomerulus or to initiate the formation of new, segregated glomeruli.

In addition to flow cytometry and electron microscopy, we have also tried to distinguish neuroblasts and glomus cells at the molecular level by performing quantitative PCRs. From all significant markers tested, the ones displaying the largest differences are shown in Fig EV4. mTH⁺/HNK⁺ cells express genes typical of immature neuroblasts, such as sodium channels (Scn9a; see below), neural developmental genes (Ntng1) [25], including sympathoadrenal lineage (Ascl1) [26], or neuroblast surface markers (Ncam2) [27]. On the other hand, mature TH⁺ cells express genes related to metabolism such as phosphofructokinase (Pfkp) [28], related to paracrine signaling such as an interleukin receptor (Il20ra), or related to a mature neuroendocrine phenotype such as the endopeptidase Pcsk6 [29] or the vesicle monoamine transporter VMAT (Slc18a1) [30].

Pre-differentiated mTH⁺/HNK⁺ neuroblasts acquire acute responsiveness to hypoxia during maturation to glomus cells

Despite differences in cell physical parameters and ultrastructure described above, CB neuroblasts (mTH⁺/HNK⁺) exhibited electrophysiological properties that, in most respects, were similar to those observed in mature (TH⁺) glomus cells (Fig 5). Both cell types showed a similar density of voltage-dependent Ca²⁺ channels; however, the amplitude (current density) of K⁺ currents was significantly larger in neuroblasts (Fig 5A–F). Most (> 80%) mTH⁺/HNK⁺ neuroblasts also showed large fast inward Na⁺ currents, a sign of cellular immaturity, which were present in < 25% of mature glomus cells (Fig 5C and G). In solid agreement with the electron microscope studies and flow cytometry data, cell capacitance, which is proportional to membrane surface area, was smaller in mTH⁺/HNK⁺ neuroblasts than in mature TH⁺ glomus cells (Fig 5H). Input resistance was similar between both cell types (Fig 5I).

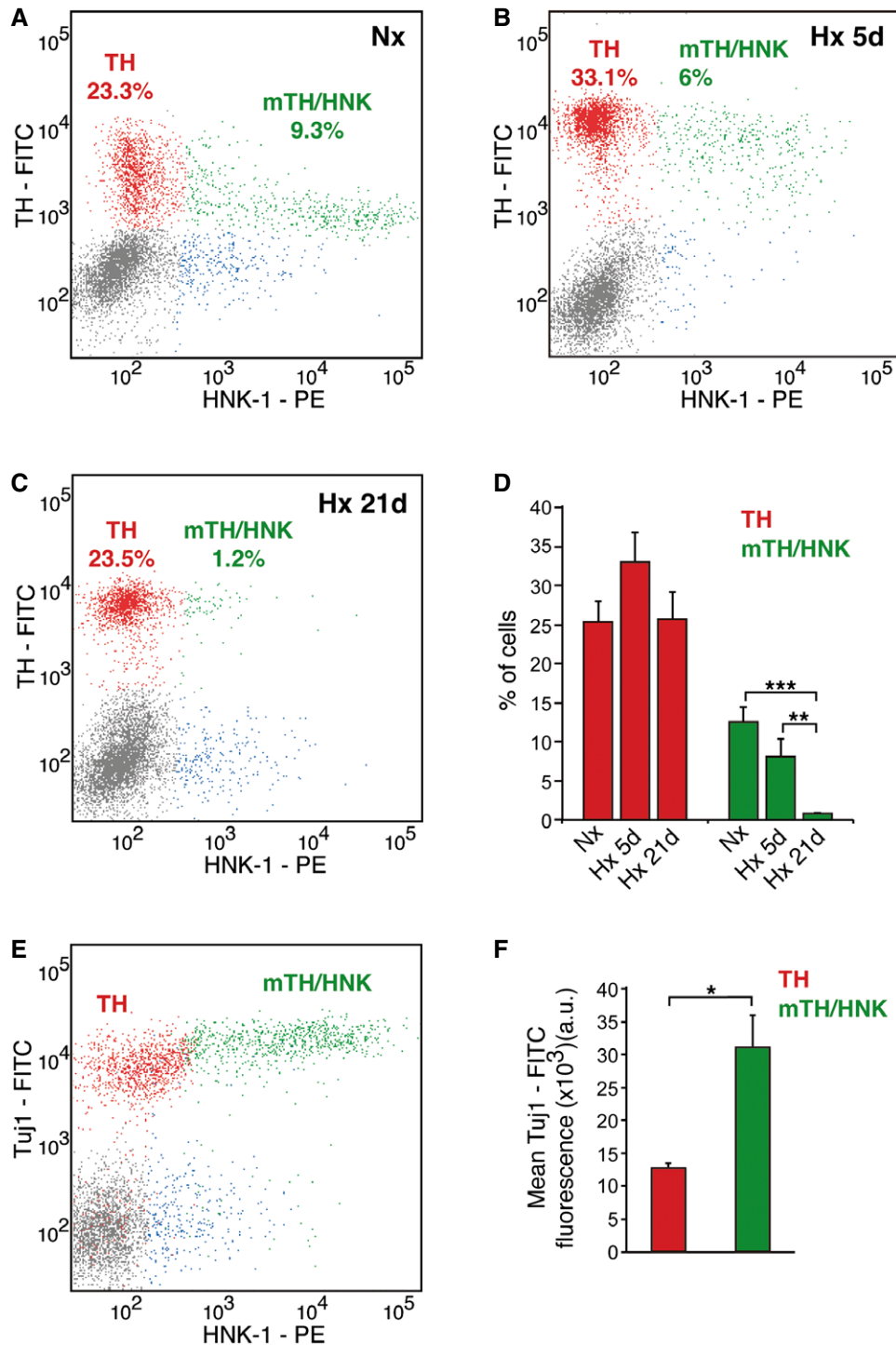


Figure 3. mTH⁺/HNK⁺ cells are immature CB neuroblasts.

A–C Flow cytometric analysis of dispersed CB cells from normoxic (Nx), 5d hypoxic (Hx), or 21d hypoxic (Hx) rats, stained for TH and HNK-1. Note how mTH⁺/HNK⁺ cells convert into TH⁺/HNK⁻ mature glomus cells upon exposure to hypoxia.

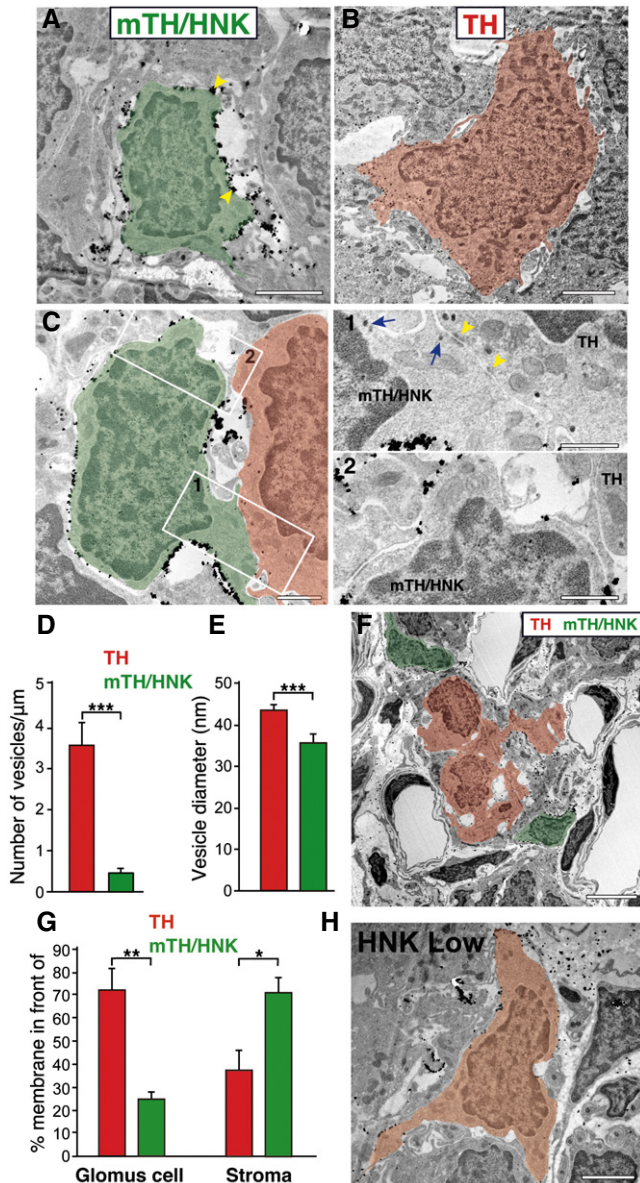
D Quantification of the flow cytometry analysis shown in (A–C) ($n = 5\text{--}7$ rats per group).

E Flow cytometry analysis of Tuj1 expression in dispersed CB cells from normoxic animals. Note how mTH⁺/HNK⁺ cells express higher levels of Tuj1 than mature TH⁺/HNK⁻ cells, confirming their immature phenotype.

F Quantification of the mean Tuj1 expression in TH⁺/HNK⁻ mature glomus cells versus mTH⁺/HNK⁺ immature neuroblasts ($n = 3$ independent experiments with a total of 10 rats).

Data information: Data in bar graphs are presented as mean \pm SEM. * $P < 0.05$, ** $P < 0.01$, *** $P < 0.001$ (Student's t -test).

Source data are available online for this figure.



Prospectively isolated CB glomerus cells and neuroblasts showed increased cytosolic $[\text{Ca}^{2+}]$ and quantal dopamine release in response to direct membrane depolarization with high external K^+ (Fig 6), which indicates that both cell classes contain functional Ca^{2+} channels that can support exocytosis (see Fig 5C and D) [12,31]. However, the size and number of individual secretory events elicited during repeated exposure to high external K^+ were clearly smaller in neuroblasts compared to glomerus cells (Fig 6A–C). These observations, consistent with the data observed in the electron microscopy studies described above (see Fig 4), further suggest that the number of vesicles and catecholamine content per vesicle are characteristics associated with the process of neuroblast maturation into glomerus cells. In addition to their response to high K^+ , mature TH^+ cells also showed an elevation of cytosolic Ca^{2+} in response to hypoxia and hypoglycemia (Fig 6D), which are characteristic responses of chemoreceptor cells [31–33]. In contrast to mature glomerus cells, less than 25% of the recorded neuroblasts

Figure 4. Electron microscopy of $\text{mTH}^+/\text{Hnk1}^+$ CB neuroblasts.

- A** Electron micrograph of a normoxic CB section after immunostaining with gold particles against HNK-1 expression. A typical HNK-1⁺ cell ($\text{mTH}/\text{Hnk1}$) is depicted in green pseudocoloring, with gold particles present all around its plasma membrane (yellow arrowheads). Scale bar: 2 μm .
- B** Electron micrograph showing a typical mature CB glomerus cell (TH) in red pseudocoloring, which is negative for the HNK-1 staining. Note how the HNK-1⁺ cell shown in (A) is smaller in size and has a thinner cytoplasm than the mature glomerus cell shown in (B). Scale bar: 2 μm .
- C** Detail of an HNK-1⁺ immature neuroblast (green) in close proximity to a mature glomerus cell (red). The areas of cell-to-cell contact have been boxed and augmented in (1) and (2). Electron-dense areas of contact can be observed (yellow arrowhead), and an increased number of larger secretory vesicles can also be detected in the mature glomerus cell. Often, prolongations of third cellular elements, as shown in (2), can be observed between the two types of cells. Scale bars: 1 μm .
- D, E** Quantification of the number of vesicles per membrane unit length, and the size of vesicles, in both mature glomerus cells (TH) and HNK-1⁺ immature neuroblasts ($\text{mTH}/\text{Hnk1}$) ($n = 31$ mature and 33 immature neuronal cells from three different normoxic rats).
- F** Low magnification electron micrograph of a normoxic CB stained for HNK-1 expression, with positive cells ($\text{mTH}/\text{Hnk1}$ neuroblasts) in green pseudocoloring and negative glomerus cells (TH) pseudocolored in red, to highlight the typical peripheral location of HNK-1⁺ neuroblasts within CB glomeruli. Scale bar: 5 μm .
- G** Quantification of the percentage of membrane surface from TH cells (red bars) or $\text{mTH}/\text{Hnk1}$ cells (green bars) located in front of a glomerus cell (TH cell) or in front of cell-free stroma. TH cells show a great percentage of their membrane in front of other TH cells (72.6% of the TH cell surface; measured in nine cells from three animals), as expected by their location inside the glomerulus. However, $\text{mTH}/\text{Hnk1}$ cell surface is mostly in front of cell-free stroma, compatible with a peripheral position of these cells within the glomeruli ($n = 5$ cells from three different rats).
- H** Electron micrograph of a carotid body section from a normoxic rat after immunostaining with gold particles against HNK-1 expression. The image shows a typical cell (pseudocolored in orange) that presents low levels of the HNK-1 marker. Scale bar: 2 μm .

Data information: Data in bar graphs are presented as mean \pm SEM.

* $P < 0.05$, ** $P < 0.01$, *** $P < 0.001$ (Student's t -test).

Source data are available online for this figure.

responded to hypoxia, and in those that did respond, the Ca^{2+} signal amplitude was $\sim 50\%$ of that recorded in TH^+ mature cells (Fig 6D–F). However, responsiveness to hypoglycemia was almost fully developed in neuroblasts (Fig 6D, G and H). NAD(P)H accumulation during hypoxia, a characteristic response of O_2 -sensitive mature glomerus cells [34], was also drastically decreased in the neuroblast population (Fig 6I and J). Taken together, these single-cell functional studies indicate that, although neuroblasts are already quite specialized cells, with fully developed Ca^{2+} channel expression and sensitivity to hypoglycemia, as well as having the ability to partially support Ca^{2+} -dependent exocytotic transmitter release, their conversion into glomerus cells requires further maturation of the neurosecretory machinery and full development of responsiveness to hypoxia.

Pharmacological modulation of CB neuroblast activation and differentiation into mature glomerus cells

As shown above, CB neuroblasts *in vivo* are quiescent in normoxia and become activated when animals are exposed to hypoxia. A similar behavior was observed in isolated $\text{mTH}^+/\text{Hnk1}^+$ cells

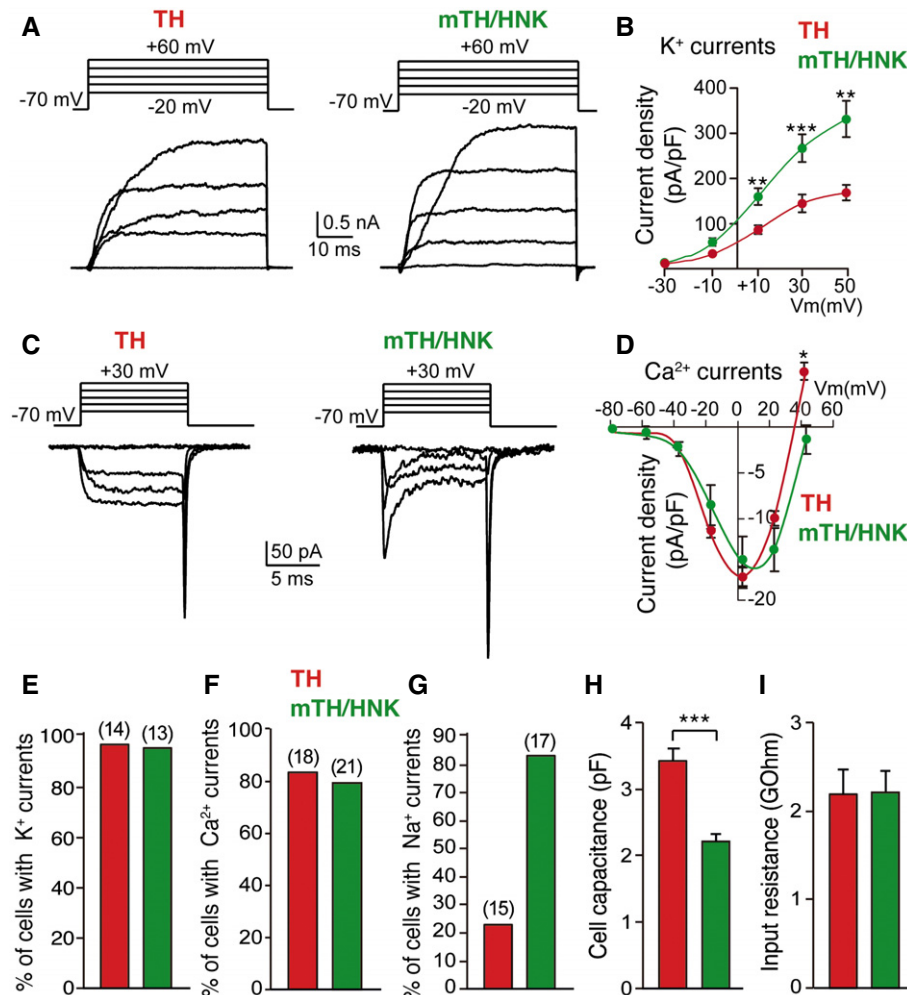


Figure 5. Electrophysiological parameters of CB mature glomus cells and neuroblasts.

- A Voltage-gated ionic outward currents elicited by depolarizing voltage steps, using the whole-cell configuration of the patch-clamp technique, on both mature glomus cells (TH) and neuroblasts (mTH/HNK), sorted alive by flow cytometry (see Fig EV2).
- B Current density measurements of outward potassium currents recorded from mature glomus cells (TH; $n = 14$ cells) and neuroblasts (mTH/HNK; $n = 13$ cells), illustrating a higher potassium channel density in immature mTH⁺/HNK⁺ cells. Data are presented as mean \pm SEM.
- C Voltage-gated ionic inward currents recorded with the whole-cell configuration of the patch-clamp technique in both mature glomus cells (TH) and neuroblasts (mTH/HNK). Note the absence of fast-activating sodium currents in mature neuronal cells.
- D Current-to-voltage relationship of inward calcium currents in both mature glomus cells (TH; $n = 18$ cells) and neuroblasts (mTH/HNK; $n = 21$ cells), reflecting the absence of important differences between the two. Data are presented as mean \pm SEM.
- E–G Quantification of the percentage of mature glomus cells (TH) and neuroblasts (mTH/HNK) displaying different ionic currents (number of total cells studied is indicated between brackets).
- H Cell capacitance measured by patch clamp in mature glomus cells (TH; $n = 29$ cells) and neuroblasts (mTH/HNK; $n = 30$ cells), confirming the smaller size of the latter.
- I Input resistance measured by patch clamp in both mature glomus cells ($n = 29$) and neuroblasts ($n = 30$).

Data information: Data in bar graphs of panels (E), (F), and (G) are presented as the sum of cells presenting the indicated ion currents among total cells studied. Data in bar graphs of panels (H) and (I) are presented as mean \pm SEM. * $P < 0.05$, ** $P < 0.01$, *** $P < 0.001$ (Student's t -test). Cells used for the analysis in this figure were obtained in three independent experiments with a total of 11 rats. Source data are available online for this figure.

in vitro, as the number of neuroblasts that became O₂-sensitive markedly increased in cell cultures maintained under hypoxic conditions (3% O₂) for 24–48 h (Fig EV5A–C, E and F). As mature (TH⁺) glomus cells are located near mTH⁺/HNK⁺ neuroblasts (see Fig 4 above), we considered the possibility that, in addition to the intrinsic effect of hypoxia (corroborated by HIF2 α

stabilization shown in Fig EV3D–F), transmitters released from glomus cells during exposure to hypoxia *in vivo* can activate neuroblast differentiation into mature cells. Among the several substances employed to test for this, the most potent and reproducible effects were obtained with ATP and acetylcholine (ACh), which are well-known transmitters stored in glomus cells that

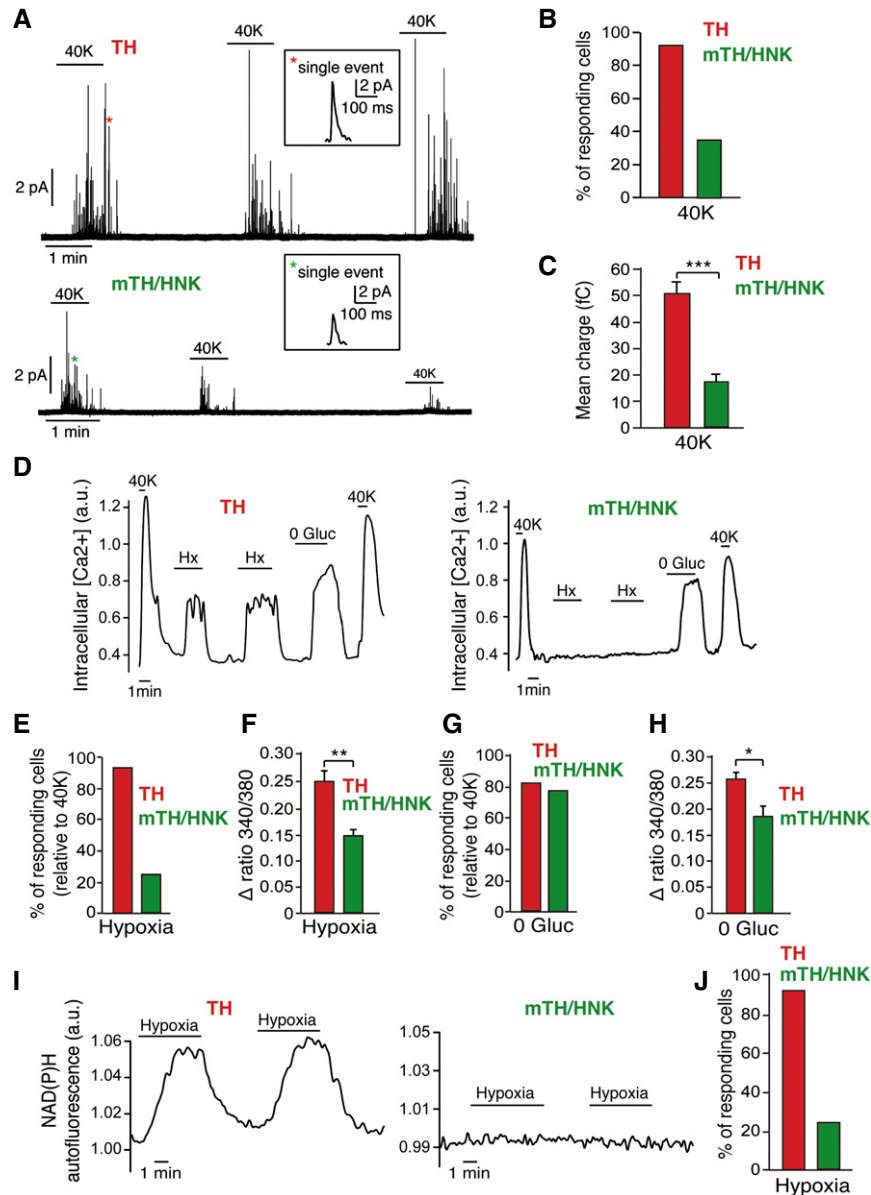


Figure 6. Functional properties of CB neuroblasts and mature glomus cells.

A Amperometric recordings of single exocytotic events from mature glomus cells (TH) or neuroblasts (mTH/HNK) in response to depolarization by extracellular solution containing high potassium. Single vesicle fusion events are shown in the insets.

B Quantification of the percentage of cells responding to high potassium as recorded by amperometry ($n = 25$ total TH⁺ cells and 26 total mTH⁺/HNK⁺ cells).

C Quantification of the mean charge of single exocytotic events from both mature glomus cells ($n = 266$ spikes from six cells) and neuroblasts ($n = 221$ spikes from six cells). The smaller charge of single fusion events from mTH⁺/HNK⁺ cells confirms their immature phenotype, in agreement with the electron microscopy data.

D Increases in intracellular calcium concentration in response to different stimuli, measured by changes in the fluorescence of the calcium indicator FURA-2. Note how CB neuroblasts (mTH/HNK) are responsive to some stimuli such as hypoglycemia (0 Gluc) or high potassium (40K) but not to others such as hypoxia (Hx).

E Percentage of cells responding to hypoxia (Hx) ($n = 117$ TH⁺ and 193 mTH⁺/HNK⁺ cells).

F Quantification of the magnitude of the response to hypoxia in both mature glomus cells (TH; $n = 108$ cells) and neuroblasts (mTH/HNK; $n = 48$ cells).

G Percentage of cells responding to hypoglycemia (0 Gluc) ($n = 48$ TH⁺ and 59 mTH⁺/HNK⁺ cells).

H Quantification of the magnitude of the response to 0 Gluc in both mature glomus cells (TH; $n = 42$ cells) and neuroblasts (mTH/HNK; $n = 47$ cells).

I Monitoring of NAD(P)H autofluorescence generated by mitochondria in response to hypoxia in both mature glomus cells (TH) and neuroblasts (mTH/HNK). Note the absence of a response by neuroblasts.

J Quantification of cells responding to hypoxia, as measured by recordings of NAD(P)H autofluorescence ($n = 117$ TH⁺ and 193 mTH⁺/HNK⁺ cells).

Data information: Data in bar graphs of panels (B), (E), (G), and (J) are presented as the sum of responding cells among total cells studied. Data in bar graphs of panels (C), (F), and (H) are presented as mean \pm SEM. * $P < 0.05$, ** $P < 0.01$, *** $P < 0.001$ (Student's *t*-test). 40K = 40 mM extracellular potassium chloride. Cells used for the analysis in panels (A), (B), (C), (I), and (J) were obtained in four independent experiments with three rats each. Cells used for the analysis in panels (D), (E), (F), (G), and (H) were obtained in four independent experiments with a total of 13 rats.

Source data are available online for this figure.

participate in chemoreceptor cell-afferent fiber synaptic communication [35]. Isolated mTH^+/HNK^+ cells acutely responded with increased cytosolic $[Ca^{2+}]$ to the application of purinergic agonists (UTP) more frequently than TH^+ cells (Fig 7A–C). CB neuroblasts appeared to be more sensitive to UTP than to ATP, and these responses were blocked by PPADS (Fig 7A–C), which suggests that P2Y metabotropic receptors were the most abundant in mTH^+/HNK^+ cells. However, immunocytochemical studies showed that P2X ionotropic receptors (which are preferentially activated by ATP) were also present in this cell subpopulation (Fig 7D). Indeed, PCR studies on enriched sorted cell subpopulations showed that several P2Y and P2X receptor mRNA species are present in TH^+ as well as in mTH^+/HNK^+ cells (Fig 7E). Application of ACh systematically elicited an increase in cytosolic $[Ca^{2+}]$ both in mature glomus cells and in pre-differentiated neuroblasts (Fig 7A and C). In agreement with these observations, the incubation of prospectively isolated mTH^+/HNK^+ cells in media with ATP, UTP, or ACh resulted in a marked increase in their maturation into O_2 -sensitive cells (Figs 7F and G, and EV5D–F). These data indicate that ATP and ACh signaling could play an important role in CB neuroblast fast proliferation and maturation. In order to further prove mature cell-neuroblast communication, we performed experiments in which neuroblasts were exposed to mature TH^+ cell-conditioned medium for several hours. However, these experiments yielded unclear results probably due to the excessive dilution of secreted factors in the conditioned medium (data not shown).

Discussion

Pre-differentiated neuroblasts in the adult carotid body

The CB contains neural crest-derived stem cells, which can support growth of the organ [12,13]. However, several histological studies using cell cycle markers (such as PCNA or Ki67) and anti-TH antibodies have suggested that neuron-like glomus cells, the main cell type in CB parenchyma, can proliferate [5,16,19]. Our data provide a novel perspective to this process, as we show that mature glomus cells do not proliferate, but rather we demonstrate the existence in the CB of quiescent, pre-differentiated TH^+ neuroblasts. This is a cell type without precedence in the adult PNS, as it can divide and fully differentiate into mature post-mitotic glomus cells to accelerate the process of adaptation to hypoxia. As both neuroblasts and glomus cells are TH^+ , it is for this reason that they were not distinguished in previous immunocytochemical analyses. The existence of two glomus cell classes in the CB had, however, been suggested in previous morphometric studies [36–38]. Interestingly, one of the cell subtypes reported in those studies, with a smaller size and a reduced number and volume of secretory vesicles, as well as a peripheral location within glomeruli [38], corresponds to the pre-differentiated neuroblasts reported here.

A typical property of CB neuroblasts is the heightened membrane expression of HNK-1, a glycoepitope reported to be a marker for neural crest-derived progenitors [39] and other neural stem cells [40]. Consistent with our data, the expression of HNK-1 has also been described in glomus cell precursors during development of the avian CB [41]. HNK-1 is usually associated with

extracellular cell adhesion molecules, which are involved in cell migration, recognition, and synaptic plasticity [42]. The role of HNK-1 in CB neuroblasts is unknown, although this marker allowed us to prospectively separate CB neuroblasts from mature glomus cells and to analyze in detail the different functional properties of these two cell types. Many of the functional characteristics of glomus cells, such as the presence of voltage-dependent Na^+ , K^+ , and Ca^{2+} channels and a relatively high level of TH expression, are already well represented in neuroblasts, suggesting that they have undergone a considerable degree of functional maturation. Indeed, CB neuroblasts, although unresponsive to acute hypoxia, are activated by low glucose, a chemoreceptive response typical of glomus cells, which, as further confirmed here, is not directly related to sensitivity to low PO_2 [32–34]. Therefore, responsiveness to hypoxia and the completion of dopaminergic secretory vesicle biogenesis are two major cell functions that distinguish glomus cells from CB neuroblasts.

Carotid body fast neurogenesis

The CB is a neurogenic center in the PNS that, similar to the subventricular zone (SVZ) or the hippocampal dentate gyrus (DG) in the brain, contains glia-like neural stem cells [12,43]. In normoxic conditions, CB stem cells are quiescent; however, upon exposure to sustained hypoxia, they convert into nestin⁺ proliferating intermediate progenitors, which then differentiate into glomus cells as well as other cell classes supporting organ growth [12,44]. In many aspects, this “slow” CB neurogenesis, which takes several days to complete, mimics neurogenesis in the central niches, although neuroblasts, or immature neurons, typically described in SVZ and DG (type A and type D cells, respectively) [45–47] had not previously been reported as such in the CB. Similar to neuroblasts in the central niches, the newly identified CB neuroblasts are Tuj1⁺, electrically excitable, and contain secretory vesicles; however, the fact that they can switch from quiescence to maturation in only few hours is a property not shared by cells in other neurogenic niches. Central neurogenesis depends on a continuous, although adjustable, sequence of events during which neuroblasts arising from intermediate progenitors immediately enter into a slow maturation process to become neurons [45–49]. In the SVZ, for example, neuroblasts migrate through the rostral migratory chain to become mature neurons at the olfactory bulb, a process that takes about 2 weeks. In the hypoxic CB, “slow neurogenesis” occurs in parallel with “fast neurogenesis”, which depends on pre-existing quiescent neuroblasts that can evolve into mature functional O_2 -sensitive cells in less than 24–48 h.

Similar to neural stem cells and intermediate progenitors [50], CB stem cells are relatively insensitive to changes in PO_2 [13]. CB “slow neurogenesis” *in vivo* is triggered by hypoxia due to the existence of abundant chemical synapses between glomus and stem cell membranes. In this way, transmitters (such as endothelin-1) released from the O_2 -sensitive mature glomus cells induce the proliferation of CB progenitors [13]. In this report, we show that hypoxia can accelerate the maturation of CB neuroblasts *in vitro*, possibly due to the induction of TH and other O_2 -regulated genes participating in this process. However, we have also observed that mature glomus cells and neuroblasts are in proximity (and even form occasional synapse-like junctions) and that

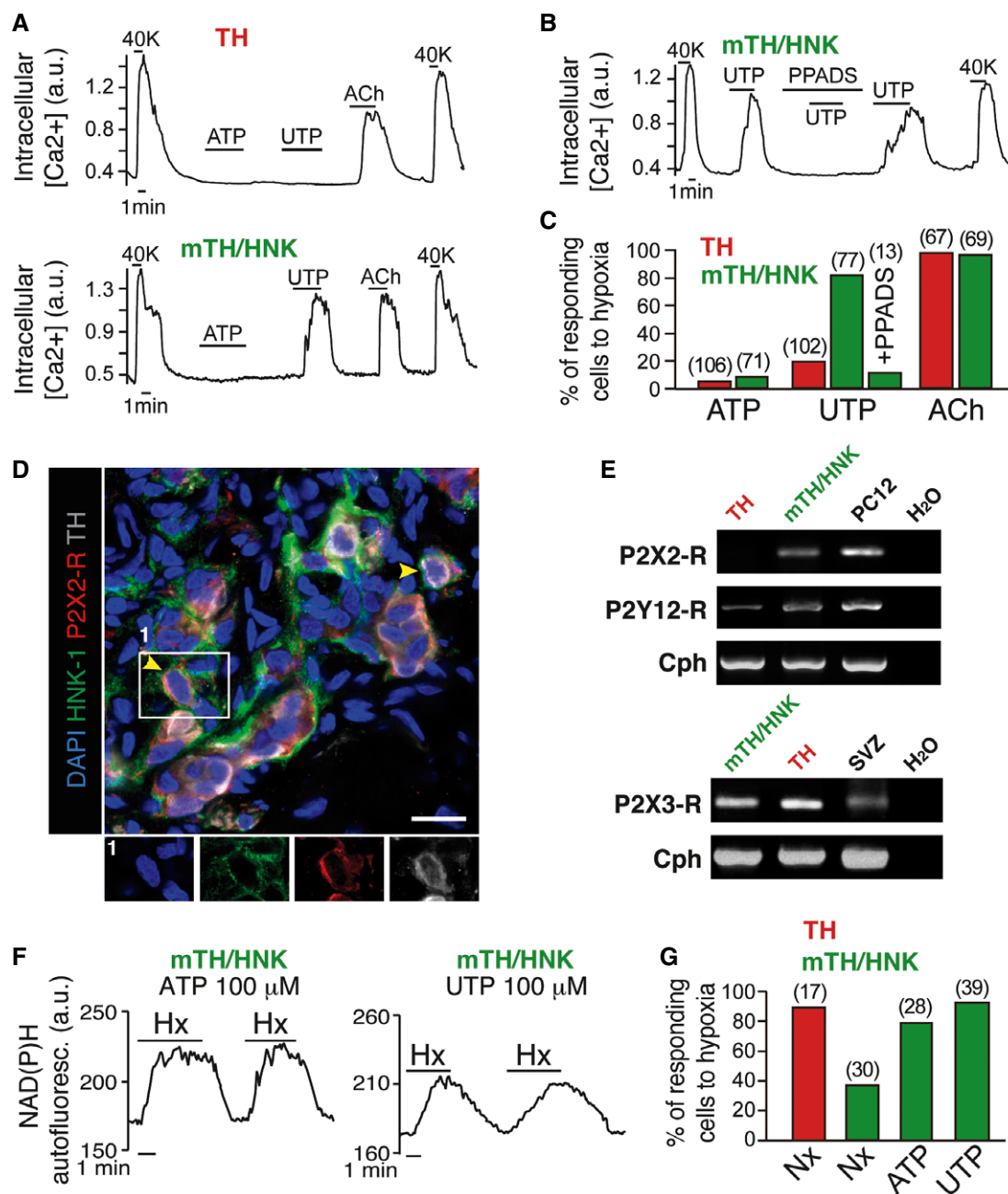


Figure 7. Purinergic and cholinergic signaling accelerates neuroblast mobilization.

- A** Intracellular calcium concentration measurements in mature glomus cells (TH) and neuroblasts (mTH/HNK) in response to purinergic (ATP and UTP) and cholinergic (acetylcholine, ACh) agonists. 40K = 40 mM extracellular potassium chloride.
- B** Intracellular calcium concentration recording from a CB neuroblast (mTH/HNK), showing inhibition of the response to UTP by the purinergic receptor blocker PPADS. 40K = 40 mM extracellular potassium chloride.
- C** Quantification of cells responding to different purinergic and cholinergic agonists (number of total cells studied is indicated between brackets). Note how CB neuroblasts respond better to the more potent purinergic agonist UTP.
- D** Histological immunodetection of purinergic receptor P2X2 expression in CB neuroblasts (mTH⁺/HNK-1⁺). Scale bar: 25 μ m.
- E** RT-PCR detection of expression of different ionotropic and metabotropic purinergic receptors in both mature glomus cells (TH) and neuroblasts (mTH/HNK).
- F** Increases in mitochondrial NAD(P)H in response to hypoxia in CB neuroblasts incubated with ATP or UTP for 24–48 h, demonstrating maturation induced by purinergic signaling.
- G** Quantification of hypoxia-responsive cells, as measured by NAD(P)H levels, after incubation for 24–48 h in the indicated conditions (number of total cells studied is indicated between brackets).

Data information: Data in bar graphs are presented as the sum of responding cells among total cells studied. Cells used for the analysis in panels (A–C), (F), and (G) were obtained in eight independent experiments with four rats each.

Source data are available online for this figure.

ACh and ATP, which are well-known transmitters released from glomus cells during hypoxia [35,51], are potential stimulants of neuroblast maturation. Interestingly, a high density of ACh receptors in the “small” glomus cells was described in previous morphometric studies [36]. In addition, ATP signaling has been implicated in the proliferation and maturation of neural progenitors [52] as well as in SVZ neuroblast migration and survival in response to ischemic insults [53]. Therefore, our observations further support the notion that mature neurons modulate neurogenesis through chemical signals acting on progenitors and on pre-differentiated neuroblasts [54], a concept optimally represented in the organization of the CB niche.

In addition to its action as a transmitter at the chemosensory cell-afferent nerve synapse, ATP released from glomus cells is known to exert paracrine interactions with glia-like (type II) cells and other elements in the CB glomerulus [55–57]. Ionotropic P2X receptors (in particular the P2X3 subtype) are predominantly expressed in the terminals of petrosal sensory neurons at the glomus cell-afferent fiber synapse, whereas metabotropic P2Y receptors seem to be more abundant in glia-like stem cells. The single-cell pharmacological studies reported here indicate that P2Y agonists activate CB neuroblast maturation into O₂-sensitive glomus cells. However, our immunohistochemical and PCR studies indicate that ionotropic P2X receptors are also expressed in immature mTH⁺/HNK⁺ cells. Further studies are warranted to examine in more detail the molecular action(s) of ATP, ACh, and other agents on quiescent neuroblasts to induce their maturation and acquisition of the O₂-sensitive phenotype.

Potential role of neuroblasts in the pathogenesis of CB over-activation: Clinical implications

The “fast neurogenesis” based on pre-existing quiescent neuroblasts described here is a process that has probably evolved to increase CB sensitivity to low PO₂ before hypertrophy of the organ takes place, thus accelerating acclimatization to hypoxia. It is possible, therefore, that the number of quiescent neuroblasts changes among mammalian species, influencing in this way their adaptability and resistance to hypoxic environments. However, an exaggerated “fast CB neurogenesis” could be maladaptive and contribute to the pathogenesis of highly prevalent medical conditions, such as refractory hypertension, sleep apnea, or left cardiac failure, presenting increased sympathetic outflow, due, at least in part, to CB over-activation [8–11]. In several of these pathologies, CB sensitization to hypoxia has been demonstrated, although the precise mechanisms are not well understood. Increased single glomus cell excitability could account for some of the observed phenomena, although it is possible that sustained CB afferent drive to the brain requires an increase in O₂-sensitive chemoreceptor cell number. Some cases of CB sensitization (e.g. in sleep apnea) occur without an apparent change in CB size or histology [58], which is compatible with the transformation of TH⁺ neuroblasts into O₂-sensitive mature glomus cells. In several animal models and in preliminary trials in human patients, CB ablation or denervation has been shown to reduce most of the effects of autonomous dysfunction [7,11], although from a translational perspective, the irreversible abolition of CB function is, obviously, not an optimal choice. Recently, an alternative pharmacological

approach based on the use of P2X3 receptor antagonists (which inhibit the glomus cell-afferent fiber synapse) was shown to have beneficial effects on hypertensive rats, although caveats have arisen regarding potential side effects [59]. Further research should explore the role of “fast” CB neurogenesis in pathological CB sensitization as well as the possible selective pharmacological inhibition of this process (e.g. with the combined use of cholinergic and/or metabotropic purinergic antagonists) while preserving CB chemosensory function.

Materials and Methods

Animals

Experiments were performed using 7- to 11-week-old Wistar rats (Harlan). Male and female animals were used in every experiment, and no differences were found between them. Rats were housed and treated according to the animal care guidelines of the European Community Council (2010/63/EU). The Animal Research Committee at the University of Seville approved all procedures.

In vivo hypoxic treatments and drug administration

Rats were chronically exposed to 10% O₂ environment for the time periods indicated, using a hermetic isobaric chamber with controlled O₂ levels and continuous monitoring of CO₂, humidity, and temperature (Coy Laboratory Products). Animals were housed in standard rodent cages, with *ad libitum* access to pellet food and water, and within a 12-h light/dark cycle room. Control rats were similarly housed in ambient air outside the chamber. To test for cell proliferation in response to hypoxia, rats were injected intraperitoneally with bromodeoxyuridine (BrdU) (50 mg/kg; Sigma) 48 h before sacrifice. BrdU was also administered in drinking water (1 mg/ml) during those 48 h. Following treatments, animals were used for immunohistochemical studies or for flow cytometry analyses.

Immunohistochemical stainings

Animals were anesthetized with ketamine (80 mg/kg) plus xylazine (10 mg/kg), intracardially perfused, and their tissue processed as described previously [13]. Immunohistochemistry procedures, including BrdU staining, were applied as previously published [12]. For HNK-1 staining, antigen retrieval was performed by covering tissue with a boiled sodium citrate solution (10 mM, pH 6) for 15 min. Sections were rinsed twice with PBS solution and then subjected to regular staining procedure. Primary antibodies: mouse-IgM anti-HNK-1 (CD57) (1:500; BD Bioscience), rat IgG2a anti-BrdU (1:200; Abcam), rabbit anti-TH (1:1,000; Novus Biological), mouse IgG1 anti-TH (1:500; Sigma), rabbit anti-Ki67 (1:200; Thermo Scientific), mouse IgG1 anti-Ki67 (1:200; BD Bioscience), and rabbit anti-P-Histone H3 (Ser28) (1:400; Cell Signaling Technology) [60]. Secondary antibodies: AlexaFluor 488-donkey-anti-rabbit-IgG (1:400; Molecular Probes), AlexaFluor 488-goat-anti-mouse-IgM (1:200; Molecular Probes), AlexaFluor 568-goat-anti-rat-IgG (1:500; Molecular Probes), AlexaFluor 568-goat-anti-mouse-IgG (1:500; Molecular Probes), AlexaFluor 568-goat-anti-rabbit-IgG (1:500;

Molecular Probes), AlexaFluor 635-goat-anti-mouse-IgG (1:500; Molecular Probes), and Cy5-goat-anti-mouse-IgG (1:200; Molecular Probes). Finally, slides were counter-stained and mounted with Fluoroshield™ with DAPI (Sigma). Images were acquired using a direct fluorescence microscope Olympus BX, a Leica TCS laser spectral-SP2-AOBS confocal microscope, or a Zeiss LSM 7 DUO confocal microscope.

Dissociation of carotid body

Rat carotid bodies were dissected from anesthetized animals and dissociated by enzymatic and mechanical treatment. Briefly, CBs were dissociated in PBS solution containing 0.6 mg/ml collagenase type II (Sigma), 0.35 U/ml porcine elastase (Calbiochem), 0.3 mg/ml trypsin (Sigma), and 10 µl/ml of 5 mM CaCl₂ solution, for 25 min at 37°C, using a shaker [61]. Once dissociated, single cells were resuspended in a staining solution composed by (for 50 ml): 44 ml L15 medium (Gibco), 0.5 ml penicillin/streptomycin (Gibco), 0.5 ml 1 M HEPES buffer (Gibco), 0.1 g BSA (Sigma), and 5 ml distilled and deionized water.

Flow cytometry analyses

Flow cytometry analyses were performed in a LSR II Fortessa Cytometer analyzer (Becton Dickinson). Once rats were exposed to hypoxic or normoxic conditions, they were anaesthetised and their carotid bodies extracted and dissociated to obtain a solution of dispersed cells (see above). The IntraPrep Permeabilization Reagent kit (Beckman Coulter) was used according to manufacturer's instructions, for cell fixation and permeabilization. As primary antibodies, we used rabbit anti-TH (1:1,000; Novus Biological), mouse-IgM anti-HNK-1 (CD57) (1:500; BD Bioscience), mouse IgG1 anti-TH (1:500; Sigma), and rabbit anti-neuron specific beta III tubulin (Tuj1) (1:1,000; Abcam). As secondary antibodies, we used FITC-goat-anti-rabbit-IgG (1:200; Jackson ImmunoResearch), PE-goat-anti-mouse-IgM (1:200; Jackson ImmunoResearch), AlexaFluor 488-donkey-anti-rabbit-IgG (1:400; Molecular Probes), and AlexaFluor 635-goat-anti-mouse-IgG (1:500; Molecular Probes).

For *ex vivo* proliferation studies, dispersed CB cells were resuspended in 200 µl of staining solution (see above) and incubated with the antibody against HNK-1 (CD57) (1:500; BD Bioscience) for 30 min on ice, followed by incubation with the secondary antibody PE-goat-anti-mouse-IgM (1:200; Jackson ImmunoResearch). Later on, intracellular staining was performed with the same samples. To do so, cells were fixed with 4% PFA for 10 min at room temperature and then rinsed with 4 ml of PBS and centrifuged at 300 g for 5 min. Cells were incubated in a blocking solution [12] for 30 min, then with the primary antibody rabbit anti-TH (1:1,000; Novus Biological) mixed with conjugated AlexaFluor 700 mouse IgG1 anti-human Ki-67 (1:200; BD Bioscience), and followed by secondary antibody FITC-goat-anti-rabbit-IgG (1:200; Jackson ImmunoResearch). Finally, cells were rinsed three times in PBS for 5 min each, with a moderate fine twister on each rinsing.

Cell sorting

Dispersed CB cells were labeled with the extracellular marker HNK-1. Sorting was performed by using either a Mo-Flo three-laser flow

cytometer (DAKO Cytomation) or a BD FACSJazz (Becton Dickinson) cell sorter. CB glomus cells were sorted by using physical parameters such as size and autofluorescence, as described in the Results section (see Results and Fig EV2). Sorted cells used for electrophysiology, cell culture, or time-lapse experiments were directly recollected in culture medium (see below). Sorted cells used for staining or flow cytometry were recollected in staining solution, and for RNA extraction, cells were directly recollected on lysis buffer, vortexed for 30 s, and stored at -80°C.

Cell culture

Proliferation assays were made with sorted cells plated in Nunc Multidish 6-well plates (Thermo Scientific), previously treated with a coating composed by 78% acetic acid 17 mM (Sigma), 20% poly-D-lysine 0.5 mg/ml (Sigma), and 2% collagen solution type 1 (Sigma). Culture medium was previously described in our laboratory [13] as complete medium, composed by D-MEM:F-12 (Gibco), 15% FBS (Gibco), 1% N2 supplement (Gibco), 2% B27 supplement (Gibco), 1% penicillin/streptomycin (Gibco), 20 ng/ml recombinant human bFGF (R&D Systems), 20 ng/ml recombinant human IGF-1 (R&D Systems), and 20 ng/ml recombinant human EGF (R&D Systems). Experiments were performed with TH⁺ cells, mTH⁺/HNK⁺ cells, and negative cells (TH⁻/HNK⁻ cells), sorted from the same pool of CB cells, plated on different wells, and placed in controlled O₂ and CO₂ conditions (normoxia: 21% O₂, or hypoxia: 3% O₂), for 24 or 48 h. When indicated, complete medium was supplemented with ATP (100 µM; Sigma). For cell size and HNK-1 expression measurements (see Fig EV3), mTH⁺/HNK⁺ cells were cultured for 4 days with complete medium without the mitogens bFGF, IGF-1, and EGF and placed in normoxia (21% O₂) or hypoxia (3% O₂). Quantification of cell size was performed by using the FIJI/ImageJ software. Finally, all adherent cells were subjected to immunocytochemical stainings.

Immunocytochemical methods

Attached cells from cell culture or time-lapse experiments were fixed with 4% PFA for 20 min at room temperature, pre-blocked for 1 h, incubated with primary antibodies overnight at 4°C, and with secondary antibodies for 2 h at room temperature. Blocking solution and antibodies were as described for immunohistochemical methods (see above), except for rabbit anti-HIF-2 alpha/EPAS1 antibody (1:100; Novus Biological) that was only used in immunocytochemistry. Images were acquired in an inverted fluorescence microscope Olympus IX-71.

Dispersed or sorted live cells were fixed and permeabilized with the IntraPrep Permeabilization Reagent kit (Beckman Coulter) according to manufacturer's instructions. Antibodies used for staining were the same than those described above. After rinsing secondary antibodies, cells were resuspended in 200–300 µl of PBS and placed in a Shandon TPX sample chamber (Thermo Scientific) with a filter card (Thermo Scientific) and a Polysine slide (Thermo Scientific). Then, cells were centrifuged in a Cytospin 4 (Thermo Scientific) and attached to the slide. Finally, slides were counter-stained and mounted with Fluoroshield™ with DAPI (Sigma). Images were acquired in a direct fluorescence microscope Olympus BX.

Live-cell imaging

Time-lapse microscopy experiments were performed with TH⁺ and mTH⁺/HNK⁺ cells, sorted from the same pool of CB cells, and plated on different wells at very low density (1,000 cells/ml) with complete medium. To improve attachment to the plate, same coating as for cell culture (see above) was used, and cells were maintained in normoxic conditions (21% O₂) at 37°C for 24 h before starting the time-lapse course. The culture dish was then transferred to the stage of an Inverted Microscope Nikon TiE Eclipse, and recording of cell behavior was performed using Hoffmann Modulation microscopy with a 20× contrast objective.

Time-lapse recordings were performed under controlled temperature (37°C) and with maintained environmental O₂ (either 20% or 10%) and CO₂ (5%), by using an Okolab system. The camera captured 12- or 8-bit digital 1,344 × 1,024 pixels grayscale images every 15 min for 48 h. The imaged microscopic fields sized 215 × 164 μm. After recording, cells were subjected to immunocytochemical staining (see above), using rabbit anti-TH (1:1,000; Novus Biological) followed by AlexaFluor 488-donkey-anti-rabbit-IgG (1:400; Molecular Probes). One last capture on each position was taken at the inverted microscope Nikon TiE Eclipse after staining, using fluorescence emission. Images were processed with ImageJ/Fiji software.

Immunohistochemistry for electron microscopy

The electron microscopy study of HNK-1 expression in rat normoxic CB was performed using the pre-embedding immunogold method [62]. Adult normoxic rats were anesthetized and transcardially perfused with PBS-based 3% PFA (Sigma) plus 0.15% glutaraldehyde (Electron Microscopy Sciences). Carotid bifurcations were removed and further fixed in 4% PFA overnight at 4°C, then embedded in gelatin (80–100 bloom; Panreac) supplemented with 2% glutaraldehyde. Finally, 50-μm-thick slices were cut on a vibratome (VT1000S; Leica Microsystems). Sections were then collected and washed thoroughly with PBS 0.1 M. Aldehyde was inactivated, in order to perform antigen retrieval, by incubating sections in 0.1% sodium borohydride (Sigma) in PB for 15 min at RT. After washing in PB, tissue sections were permeabilized in 0.05% Triton X-100 in PB 30 min at RT. Sections were then washed and incubated in Aurion Blocking Solution (Aurion) during 1 h at 4°C. After blocking, sections were incubated overnight in mouse-IgM anti-HNK-1 (BD Bioscience) diluted 1:100 in PBS, with the addition of 0.2% BSA-cTM (Aurion). After several washes in PBS-0.2% BSA-cTM, sections were incubated in 1:100 ultra small gold-conjugated secondary antibody (anti-mouse-IgM; Aurion) in PBS-0.2% BSA-cTM overnight at 4°C. After that, sections were washed and post-fixed with 2.5% glutaraldehyde in PB for 2 h. Sections were washed in double-distilled water, followed by silver enhancement of the nanogold particles with SE-EM enhancement mixture (Aurion), for 1 h and 30 min at RT. CB sections were then treated with aqueous 0.5% OsO₄ for 15 min at RT and block stained with 2% uranyl acetate. Sections were then dehydrated in ethanol series (40, 50, 70, 80, 95, and 100% ethanol) before infiltrating and embedding in Epon resin (Electron Microscopy Sciences). Semi-thin sections (1 μm thick) were cut with a glass knife.

Ultrathin sections (60 nm) were cut with a diamond knife and examined at Zeiss Libra 120 electron microscope. Pictures of both mTH⁺/HNK-1⁺ and TH⁺ type I cells were taken at 4 K and 10 K magnification for estimation of cell size and dense core vesicle diameter, respectively. Type I cells were distinguished using typical morphological hallmarks such as size, round, and centrally placed nucleus with a single prominent nucleolus [24], dense core vesicles, high cytoplasm complexity, and plentiful and branched mitochondria [23]. Quantifications were performed using ImageJ software.

Electrophysiological recordings

Electrophysiological recordings were performed in single cells obtained from rat carotid bodies dispersed and sorted as described above. Cells were plated on poly-L-lysine-treated glass coverslips with complete medium (see above) at 37°C in an incubator in normoxic conditions until use. For chronic experiments, cells were exposed to hypoxic (3%) or normoxic conditions, and complete medium was supplemented with ATP (100 μM; Sigma), UTP (100 μM; Sigma), or ACh (10 μM; Sigma) for 24–48 h.

Amperometric recording of single-cell catecholamine secretion

Cells were recorded 4–7 h after dispersion. They were transferred to a recording chamber and continuously perfused with a control solution containing (in mM) 117 NaCl, 4.5 KCl, 23 NaHCO₃, 1 MgCl₂, 2.5 CaCl₂, 5 glucose, and 5 sucrose. In high K⁺ solutions, NaCl was replaced by KCl equimolarly. Solutions were bubbled with a gas mixture of 5% CO₂, 20% O₂, and 75% N₂ (O₂ tension ~145 mmHg). Osmolality of solutions was ~300 mOsmol/kg, and pH was 7.4. All experiments were carried out at 30–33°C. Secretory events were recorded with a 5 μm carbon-fiber electrode positioned under visual control. Cumulative secretion signal was the sum of time integral values of successive amperometric events [63]. Amperometric currents were recorded with an EPC-10 patch-clamp amplifier (HEKA Electronics, Lambrecht/Pfaltz, Germany), filtered at 100 Hz, and digitized at 250 Hz before storage on computer. Data acquisition and analysis were done with PatchMaster software (HEKA Electronics) and Igor 6. Secretion rate (femtoCoulombs (fC)/min) was calculated as the amount of charge transferred to the recording electrode during a given period of time.

Patch-clamp recordings

Macroscopic ionic currents were recorded from dispersed rat glomus cells using the whole-cell configuration of the patch-clamp technique, as adapted to our laboratory [34]. Patch electrodes (2.5–3 MΩ) were pulled from capillary glass tubes (Kimax, Kimble Products) and fire polished on a microforge MF-830 (Narishige). Voltage-clamp recordings were obtained with an EPC-10 patch-clamp amplifier (Heka Elektronik) using standard voltage-clamp protocols designed with Patch Master software (Heka Elektronik). Unless otherwise noted, holding potential was –70 mV. Data were filtered at 10 kHz, digitized at sampling interval of 20 μs, and stored on a Macintosh computer. Offline data analysis was performed using Igor 6 and Patch Master Fit (Heka Elektronik). All experiments were conducted at 30–33°C. Macroscopic Ca²⁺, Na⁺, and K⁺ currents were recorded in dialyzed glomus cells.

Solutions used for the recording of whole-cell Na^+ and Ca^{2+} currents contained (in mM): external: 140 NaCl, 9 BaCl_2 , 2.5 KCl, 1 CaCl_2 , 10 HEPES, and 10 glucose; pH 7.4 and osmolality 300 mOsm/kg; and internal: 110 CsCl, 30 CsF, 10 EGTA, 10 HEPES, and 4 ATP-Mg; pH 7.2, and osmolality 285 mOsm/kg. The solutions used for the recording of whole-cell K^+ currents contained (in mM): external: 140 NaCl, 2.5 KCl, 10 HEPES, 10 glucose, 2.5 CaCl_2 , and 4 MgCl_2 ; pH 7.4 and osmolality 300 mOsm/kg; and internal: 80 potassium glutamate, 50 KCl, 1 MgCl_2 , 10 HEPES, 4 ATP-Mg, and 5 EGTA; pH 7.2, and osmolality 280 mOsm/kg.

Microfluorimetric measurements

For cytosolic Ca^{2+} measurements, glomus cells were first incubated in DMEM containing Fura 2-AM (2 μM ; TefLabs MW 1002) for 45 min at 37°C in a 5% CO_2 incubator. For the experiments, a coverslip with loaded cells was placed on a recording chamber mounted on the stage of an inverted microscope (Axiovert 35, Zeiss) equipped with epifluorescence and photometry. Alternating excitation wavelengths of 340 and 380 nm were used, and background fluorescence was subtracted before obtaining the F340/F380 ratio [31]. As calibration of $[\text{Ca}^{2+}]$ was not done, the relative changes in $[\text{Ca}^{2+}]$ for each experiment are given by the F340/F380 ratio. Cytosolic $[\text{Ca}^{2+}]$ signal was digitized at a sampling interval of 500 ms. All experiments were performed at room temperature (~25°C). Measurements of NAD(P)H autofluorescence were taken using a non-ratio metric protocol. NADH was excited at 360 nm and measured at 460 nm. Background fluorescence was subtracted in all the experiments.

RNA amplification, RT-PCR, and qPCR

Total RNA was extracted from sorted cells using a commercial kit (RNeasy MICRO kit, Qiagen), following manufacturer's instructions. RNA was amplified with GeneChip WT Pico Reagent kit, following manufacturer's instructions. For retrotranscription, cDNA was synthesized with the qScript cDNA SuperMix (Quantabio). Standard PCRs were performed using Biotaq™ DNA Polymerase (Bioline), in a T-professional Trio Thermocycler (Biometra). Primers used for the reactions amplified the following genes: P2X2 and P2X3 [64], P2Y12 [65], and cyclophilin as housekeeping [66]. Primer sequences and PCR product sizes are shown in the following table:

Subtype	Primer sequence (5'–3')	PCR product size (bp)
P2X2	(s)GAATCAGAGTCAACCCCAA (as)TCACAGGCCATCTACTTGAG	375
P2X3	(s)TTGAGGGTAGGGGATGTGGT (as)GCTGATAATGGTGGGATGA	326
P2Y12	(s)TCCCATTGCTCTACACTGTC (as)TGTCCTTTCTTTATTTC	895
Cyclophilin	(s)GTCTCTTTTCGCCGCTTGCTG (as)GCTCATGCCTTCTTACCTCC	437

Quantitative PCRs were performed using TaqMan specific probes for selected genes (Scn9a, Ntn1, Asc1, Ncam2, Slc18a1, Il20ra, Pfkfb, Pcsk6, and Hprt1) and the TaqMan Gene Expression Master Mix (Applied Biosystems).

Statistical analysis

Data are presented as mean \pm SEM. Statistical comparisons in this study were performed using a two-tailed Student's *t*-test with a Levene test for homogeneity of variances. Normal distribution was assessed by Shapiro–Wilk test. Differences were considered significant with a *P*-value of **P* < 0.05, ***P* < 0.01, or ****P* < 0.001.

Expanded View for this article is available online.

Acknowledgements

We thank María José Castro, Juan Luis Ribas, Francisco Vega, José Luis Nieto, Ignacio Arias-Mayenco, and Sergio Valverde for technical assistance. This work was supported by grants from the Botín Foundation, the Spanish Ministry of Economy and Competitiveness (SAF Program: SAF2012-39343, SAF2013-48535-P, and SAF2016-80412-P, co-funded by FEDER funds), the Spanish Ministry of Health (ISCIII PIE13/0004), and the European Research Council (ERC Starting Grant to RP and ERC Advanced Grant to JL-B).

Author contributions

VS, PG-R, and VA performed experiments and contributed to the design of the study. JL-B and RP designed the study, wrote the manuscript, and supervised the project.

Conflict of interest

The authors declare that they have no conflict of interest.

References

- Hempleman SC, Warburton SJ (2012) Comparative embryology of the carotid body. *Respir Physiol Neurobiol* 185: 3–8
- Lopez-Barneo J, Ortega-Saenz P, Gonzalez-Rodriguez P, Fernandez-Aguera MC, Macias D, Pardal R, Gao L (2016) Oxygen-sensing by arterial chemoreceptors: mechanisms and medical translation. *Mol Aspects Med* 47–48: 90–108
- Arias-Stella J, Valcarcel J (1976) Chief cell hyperplasia in the human carotid body at high altitudes; physiologic and pathologic significance. *Hum Pathol* 7: 361–373
- Wang ZY, Bisgard GE (2002) Chronic hypoxia-induced morphological and neurochemical changes in the carotid body. *Microsc Res Tech* 59: 168–177
- Wang ZY, Olson EB Jr, Bjorling DE, Mitchell GS, Bisgard GE (2008) Sustained hypoxia-induced proliferation of carotid body type I cells in rats. *J Appl Physiol* 104: 803–808
- Heath D, Smith P, Jago R (1982) Hyperplasia of the carotid body. *J Pathol* 138: 115–127
- Del Rio R, Andrade DC, Lucero C, Arias P, Iturriaga R (2016) Carotid body ablation abrogates hypertension and autonomic alterations induced by intermittent hypoxia in rats. *Hypertension* 68: 436–445
- Del Rio R, Marcus NJ, Schultz HD (2013) Carotid chemoreceptor ablation improves survival in heart failure: rescuing autonomic control of cardiorespiratory function. *J Am Coll Cardiol* 62: 2422–2430
- Paton JF, Sobotka PA, Fudim M, Engelman ZJ, Hart EC, McBryde FD, Abdala AP, Marina N, Gourine AV, Lobo M, et al (2013) Response to role of the carotid body in obesity-related sympathoactivation. *Hypertension* 61: e58

10. Ponikowski P, Chua TP, Anker SD, Francis DP, Doehner W, Banasiak W, Poole-Wilson PA, Piepoli MF, Coats AJ (2001) Peripheral chemoreceptor hypersensitivity: an ominous sign in patients with chronic heart failure. *Circulation* 104: 544–549
11. McBryde FD, Abdala AP, Hendy EB, Pijacka W, Marvar P, Moraes DJ, Sobotka PA, Paton JF (2013) The carotid body as a putative therapeutic target for the treatment of neurogenic hypertension. *Nat Commun* 4: 2395
12. Pardal R, Ortega-Saenz P, Duran R, Lopez-Barneo J (2007) Glia-like stem cells sustain physiologic neurogenesis in the adult mammalian carotid body. *Cell* 131: 364–377
13. Platero-Luengo A, Gonzalez-Granero S, Duran R, Diaz-Castro B, Piruat JL, Garcia-Verdugo JM, Pardal R, Lopez-Barneo J (2014) An O₂-sensitive glomus cell-stem cell synapse induces carotid body growth in chronic hypoxia. *Cell* 156: 291–303
14. Alvarez-Buylla A, Lim DA (2004) For the long run: maintaining germinal niches in the adult brain. *Neuron* 41: 683–686
15. Kriegstein A, Alvarez-Buylla A (2009) The glial nature of embryonic and adult neural stem cells. *Annu Rev Neurosci* 32: 149–184
16. Chen J, He L, Liu X, Dinger B, Stensaas L, Fidone S (2007) Effect of the endothelin receptor antagonist bosentan on chronic hypoxia-induced morphological and physiological changes in rat carotid body. *Am J Physiol Lung Cell Mol Physiol* 292: L1257–L1262
17. McGregor KH, Gil J, Lahiri S (1984) A morphometric study of the carotid body in chronically hypoxic rats. *J Appl Physiol Respir Environ Exerc Physiol* 57: 1430–1438
18. Nurse CA, Fearon IM (2002) Carotid body chemoreceptors in dissociated cell culture. *Microsc Res Tech* 59: 249–255
19. Paciga M, Vollmer C, Nurse C (1999) Role of ET-1 in hypoxia-induced mitosis of cultured rat carotid body chemoreceptors. *NeuroReport* 10: 3739–3744
20. Basch ML, Bronner-Fraser M, Garcia-Castro MI (2006) Specification of the neural crest occurs during gastrulation and requires Pax7. *Nature* 441: 218–222
21. Erickson CA, Loring JF, Lester SM (1989) Migratory pathways of HNK-1-immunoreactive neural crest cells in the rat embryo. *Dev Biol* 134: 112–118
22. Menezes JR, Luskin MB (1994) Expression of neuron-specific tubulin defines a novel population in the proliferative layers of the developing telencephalon. *J Neurosci* 14: 5399–5416
23. Bischof TJ, Stehbens WE (1966) Ultrastructure of the carotid body. *J Cell Biol* 30: 563–578
24. Ross LL (1959) Electron microscopic observations of the carotid body of the cat. *J Biophys Biochem Cytol* 6: 253–262
25. Song YS, Lee HJ, Prosser P, Itohara S, Kim E (2013) Trans-induced cis interaction in the tripartite NGL-1, netrin-G1 and LAR adhesion complex promotes development of excitatory synapses. *J Cell Sci* 126: 4926–4938
26. Kameda Y (2005) Mash1 is required for glomus cell formation in the mouse carotid body. *Dev Biol* 283: 128–139
27. Bonfanti L, Olive S, Poulain DA, Theodosis DT (1992) Mapping of the distribution of polysialylated neural cell adhesion molecule throughout the central nervous system of the adult rat: an immunohistochemical study. *Neuroscience* 49: 419–436
28. Gao L, Bonilla-Henao V, Garcia-Flores P, Arias-Mayenco I, Ortega-Saenz P, Lopez-Barneo J (2017) Gene expression analyses reveal metabolic specifications in acute O₂-sensing chemoreceptor cells. *J Physiol* 595: 6091–6120
29. Yoshida I, Koide S, Hasegawa SI, Nakagawara A, Tsuji A, Matsuda Y (2001) Proprotein convertase PACE4 is down-regulated by the basic helix-loop-helix transcription factor HASH-1 and MASH-1. *Biochem J* 360: 683–689
30. Eiden LE, Schafer MK, Weihe E, Schutz B (2004) The vesicular amine transporter family (SLC18): amine/proton antiporters required for vesicular accumulation and regulated exocytotic secretion of monoamines and acetylcholine. *Pflugers Arch* 447: 636–640
31. Ureña J, Fernandez-Chacon R, Benot AR, Alvarez de Toledo GA, Lopez-Barneo J (1994) Hypoxia induces voltage-dependent Ca²⁺ entry and quantal dopamine secretion in carotid body glomus cells. *Proc Natl Acad Sci USA* 91: 10208–10211
32. Garcia-Fernandez M, Ortega-Saenz P, Castellano A, Lopez-Barneo J (2007) Mechanisms of low-glucose sensitivity in carotid body glomus cells. *Diabetes* 56: 2893–2900
33. Pardal R, López-Barneo J (2002) Low glucose-sensing cells in the carotid body. *Nat Neurosci* 5: 197–198
34. Fernandez-Aguera MC, Gao L, Gonzalez-Rodriguez P, Pintado CO, Arias-Mayenco I, Garcia-Flores P, Garcia-Perganeda A, Pascual A, Ortega-Saenz P, Lopez-Barneo J (2015) Oxygen sensing by arterial chemoreceptors depends on mitochondrial complex I signaling. *Cell Metab* 22: 825–837
35. Zhang M, Zhong H, Vollmer C, Nurse CA (2000) Co-release of ATP and ACh mediates hypoxic signalling at rat carotid body chemoreceptors. *J Physiol* 525(Pt. 1): 143–158
36. Chen I-L, Yates RD (1984) Two types of glomus cell in the rat carotid body as revealed by alpha-bungarotoxin binding. *J Neurocytol* 13: 281–302
37. Hellstrom S (1975) Morphometric studies of dense-cored vesicles in type I cells of rat carotid body. *J Neurocytol* 4: 77–86
38. McDonald DM, Mitchell RA (1975) The innervation of glomus cells, ganglion cells and blood vessels in the rat carotid body: a quantitative ultrastructural analysis. *J Neurocytol* 4: 177–230
39. Bronner-Fraser M (1986) Analysis of the early stages of trunk neural crest migration in avian embryos using monoclonal antibody HNK-1. *Dev Biol* 115: 44–55
40. Yagi H, Yanagisawa M, Suzuki Y, Nakatani Y, Ariga T, Kato K, Yu RK (2010) HNK-1 epitope-carrying tenascin-C spliced variant regulates the proliferation of mouse embryonic neural stem cells. *J Biol Chem* 285: 37293–37301
41. Kameda Y, Yamatsu Y, Kameya T, Frankfurter A (1994) Glomus cell differentiation in the carotid body region of chick embryos studied by neuron-specific class III beta-tubulin isotype and Leu-7 monoclonal antibodies. *J Comp Neurol* 348: 531–543
42. Kizuka Y, Oka S (2012) Regulated expression and neural functions of human natural killer-1 (HNK-1) carbohydrate. *Cell Mol Life Sci* 69: 4135–4147
43. Diaz-Castro B, Pardal R, Garcia-Flores P, Sobrino V, Duran R, Piruat JL, Lopez-Barneo J (2015) Resistance of glia-like central and peripheral neural stem cells to genetically induced mitochondrial dysfunction-differential effects on neurogenesis. *EMBO Rep* 16: 1511–1519
44. Annesse V, Navarro-Guerrero E, Rodriguez-Prieto I, Pardal R (2017) Physiological plasticity of neural-crest-derived stem cells in the adult mammalian carotid body. *Cell Rep* 19: 471–478
45. Doetsch F, Caille I, Lim DA, Garcia-Verdugo JM, Alvarez-Buylla A (1999) Subventricular zone astrocytes are neural stem cells in the adult mammalian brain. *Cell* 97: 703–716
46. Kempermann G, Song H, Gage FH (2015) Neurogenesis in the adult hippocampus. *Cold Spring Harb Perspect Biol* 7: a018812

47. Seri B, Garcia-Verdugo JM, McEwen BS, Alvarez-Buylla A (2001) Astrocytes give rise to new neurons in the adult mammalian hippocampus. *J Neurosci* 21: 7153–7160
48. Aimone JB, Wiles J, Gage FH (2006) Potential role for adult neurogenesis in the encoding of time in new memories. *Nat Neurosci* 9: 723–727
49. Kohler SJ, Williams NI, Stanton GB, Cameron JL, Greenough WT (2011) Maturation time of new granule cells in the dentate gyrus of adult macaque monkeys exceeds six months. *Proc Natl Acad Sci USA* 108: 10326–10331
50. d'Anglemont de Tassigny X, Sierrol-Piquer MS, Gomez-Pinedo U, Pardal R, Bonilla S, Capilla-Gonzalez V, Lopez-Lopez I, De la Torre-Laviana FJ, Garcia-Verdugo JM, Lopez-Barneo J (2015) Resistance of subventricular neural stem cells to chronic hypoxemia despite structural disorganization of the germinal center and impairment of neuronal and oligodendrocyte survival. *Hypoxia* 3: 15–33
51. Iturriaga R, Alcayaga J (2004) Neurotransmission in the carotid body: transmitters and modulators between glomus cells and petrosal ganglion nerve terminals. *Brain Res Brain Res Rev* 47: 46–53
52. Rathbone MP, Middlemiss PJ, Gysbers JW, Andrew C, Herman MA, Reed JK, Ciccarelli R, Di Iorio P, Caciagli F (1999) Trophic effects of purines in neurons and glial cells. *Prog Neurobiol* 59: 663–690
53. Vergni D, Castiglione F, Briani M, Middei S, Alberdi E, Reymann KG, Natalini R, Volonte C, Matute C, Cavaliere F (2009) A model of ischemia-induced neuroblast activation in the adult subventricular zone. *PLoS One* 4: e5278
54. Pardal R, López-Barneo J (2016) Mature neurons modulate neurogenesis through chemical signals acting on neural stem cells. *Dev Growth Differ* 58: 456–462
55. Murali S, Nurse CA (2016) Purinergic signalling mediates bidirectional crosstalk between chemoreceptor type I and glial-like type II cells of the rat carotid body. *J Physiol* 594: 391–406
56. Piskuric NA, Nurse CA (2013) Expanding role of ATP as a versatile messenger at carotid and aortic body chemoreceptors. *J Physiol* 591: 415–422
57. Tse A, Yan L, Lee AK, Tse FW (2012) Autocrine and paracrine actions of ATP in rat carotid body. *Can J Physiol Pharmacol* 90: 705–711
58. Peng YJ, Overholt JL, Kline D, Kumar GK, Prabhakar NR (2003) Induction of sensory long-term facilitation in the carotid body by intermittent hypoxia: implications for recurrent apneas. *Proc Natl Acad Sci USA* 100: 10073–10078
59. Pijacka W, Moraes DJ, Ratcliffe LE, Nightingale AK, Hart EC, da Silva MP, Machado BH, McBryde FD, Abdala AP, Ford AP, et al (2016) Purinergic receptors in the carotid body as a new drug target for controlling hypertension. *Nat Med* 22: 1151–1159
60. Goto H, Tomono Y, Ajiro K, Kosako H, Fujita M, Sakurai M, Okawa K, Iwamatsu A, Okigaki T, Takahashi T, et al (1999) Identification of a novel phosphorylation site on histone H3 coupled with mitotic chromosome condensation. *J Biol Chem* 274: 25543–25549
61. Navarro-Guerrero E, Platero-Luengo A, Linares-Clemente P, Cases I, Lopez-Barneo J, Pardal R (2016) Gene expression profiling supports the neural crest origin of adult rodent carotid body stem cells and identifies CD10 as a marker for mesectoderm-committed progenitors. *Stem Cells* 34: 1637–1650
62. Bendayan M (2001) Tech. Sight. Worth its weight in gold. *Science* 291: 1363–1365
63. Pardal R, López-Barneo J (2002) Carotid body thin slices: responses of glomus cells to hypoxia and K(+)-channel blockers. *Respir Physiol Neurobiol* 132: 69–79
64. Prasad M, Fearon IM, Zhang M, Laing M, Vollmer C, Nurse CA (2001) Expression of P2X2 and P2X3 receptor subunits in rat carotid body afferent neurones: role in chemosensory signalling. *J Physiol* 537: 667–677
65. Hu RG, Suzuki-Kerr H, Webb KF, Rhodes JD, Collison DJ, Duncan G, Donaldson PJ (2008) Molecular and functional mapping of regional differences in P2Y receptor expression in the rat lens. *Exp Eye Res* 87: 137–146
66. Bautista L, Castro MJ, Lopez-Barneo J, Castellano A (2009) Hypoxia inducible factor-2alpha stabilization and maxi-K⁺ channel beta1-subunit gene repression by hypoxia in cardiac myocytes: role in preconditioning. *Circ Res* 104: 1364–1372